J Syst Sci Complex (2022) 35: 159–178

Stability and Hopf Bifurcation Analysis of an $(n+m)$-Neuron Double-Ring Neural Network Model with Multiple Time Delays*

XING Ruitao · XIAO Min · ZHANG Yuezhong · QIU Jianlong

DOI: 10.1007/s11424-021-0108-2
Received: 19 May 2020 / Revised: 19 August 2020

Abstract Up till the present moment, researchers have always featured the single-ring neural network. These investigations, however, disregard the link between rings in neural networks. This paper highlights a high-dimensional double-ring neural network model with multiple time delays. The neural network has two rings of a shared node, where one ring has n neurons and the other has $m+1$ neurons. By utilizing the sum of time delays as the bifurcation parameter, the method of Coates' flow graph is applied to obtain the relevant characteristic equation. The stability of the neural network model with bicyclic structure is discussed by dissecting the characteristic equation, and the critical value of Hopf bifurcation is derived. The effect of the sum of time delays and the number of neurons on the stability of the model is extrapolated. The validity of the theory can be verified by numerical simulations.

Keywords Coates' flow graph, high-dimensional, Hopf bifurcation, stability.

1 Introduction

The neural network is a nonlinear system composed of numerous neurons through extremely plentiful and distinctive connections, accordingly, it has sizeable and complex structure[1]. Neurons are the basic structure and functional unit of the neural system. The process by which neurons generate and transmit electrical impulses is considered to be a manifestation of the

XING Ruitao · XIAO Min (Corresponding author) · ZHANG Yuezhong
College of Automation and College of Artificial Intelligence, Nanjing University of Posts and Telecommunications, Nanjing 210003*, China.*
Email: ruitaoxing@163.com; candymanxm2003@aliyun.com; m13255291236@163.com.
QIU Jianlong
School of Automation and Electrical Engineering, Linyi University, Linyi 276000*, China.*
Email: qjllinyi@aliyun.com.
*This work was supported by the National Natural Science Foundation of China under Grant Nos. 61573194, 62073172, 61877033, and the Natural Science Foundation of Jiangsu Province of China under Grant No. BK20181389.
◇ *This paper was recommended for publication by Editor XIN Bin.*

discharge activity of the nervous system. The diversity of the bifurcation types and the combinations of the dynamical systems of the neuronal system makes the firing patterns of neurons copious and multiplex, which leads to the generation of involuted dynamic behaviors. Neural networks are used to simulate the dynamic behavior of the brain, and the stability of the neural network can reflect the stability of physiological mechanisms[2]. The dynamic behavior of brains will be confused once stability changes, leading to the development of nervous system diseases, such as mania. The second messenger balance mechanism is broken, leading to a decline or enhancement of brain function, which may lead to manic episodes[3, 4]. In this sense, the stability analysis of neural networks is of great significance for the treatment of mental illness.

Zieglgansberger and Tolle proposed a system biology method to probe the mechanism of neuralgia[5], thereafter, the system biology of cell signal network and gene expression regulation has existed an eventful content of neurobiology research. For another, it is universally known that the stability which is habitually inseparable from structure of neural networks should not be ignored when neurons transmit information in the concrete operation of biological and artificial neural networks. Furthermore, the nonlinear dynamics of neural networks commonly depend on the evolution of time and the interaction of spatial distribution structures. Consequently, the dynamic analysis of the double-ring neural network with time delays owns huge potential in both theoretical and practical research fields.

Since the invention of the famous Hopfield neural network[6], neural networks have received more and more attention for their rich dynamic behaviors. These behaviors include stability, multi-periodicity, bifurcation, synchronization[7] and chaos[8]. The exploration of neural networks involves many scientific fields such as medicine, biology, physiology, informatics, and computer science[9–11]. The examination of neural networks can be divided into two categories. One is the applied research, such as artificial intelligence, deep learning, knowledge engineering, expert systems, optimization combinations, unmanned vehicle[12–14]. The other is the theoretical consideration. The research results of neural basic theories and mathematical methods were applied to the establishment of neural network models for better functions and performance[15, 16]. This paper focuses on the second half, establishing a neural network model and analyze its stability.

High-dimensional Hopfield neural networks have been profoundly quested by myriad scholars in theory and application owing to its strong computing and learning capabilities. High-dimensional neural networks possess stronger approximation, faster convergence, larger storage capacity, and higher fault tolerance and storage capacity[17]. However, high-dimensional neural network models are inevitably complex in analysis and calculations. In addition, most of the existing results on the stability and bifurcation of the ring system are defective, which contain either only one ring or low dimensionality. It is so arduous to deal with double rings and high dimensionality at the same time. Therefore, it is necessary and challenging to establish the general conditions and properties of Hopf bifurcation in a double-ring high-dimensional model with time delays.

There are unavoidable time delays for the limited transmission speed when neurons process information[18]. The propagation speed of membrane potential through neurons' axons is

limited, consequently, the interaction between two coupled neurons is not instantaneous. Time delays should be explicitly included in the coupled system in order to explain this non-transient characteristic. Time delays play an important role in the coupling system that simulates real-world processes and experimental systems, including interactive lasers, real creatures and artificial neural networks[19]. Time delays may damage the stability of the system and then fail to meet our expectations[20–22]. Therefore, the time delay must be taken into account when probing the stability of a neural network. Several high-dimensional models of Hopfield neural networks have been proposed[23]. The author proved the superiority of the proposed model but the author did not consider the impact of the time delay on the system. In this paper, the sum of time delays is used as the bifurcation parameter, which is more in line with the actual situation.

The existence of ring networks has been found in many neural structures, such as motion in natural phenomena, breathing, etc., or the back and forth motion of pistons in cylinders in artificial machines[24]. Ring geometry has been widely exploited in physiological and biochemical modeling research. Many researchers have analyzed the ring model in the context of neural network theory. It has also been noted that the ring structure may be related to the development of patterns on certain animal shells and other system functions. From the perspective of physiological modeling, ring networks are eventful because they can act as basic components of more complex systems[25]. The ring neural network belongs to a class of feedback systems and possesses important biological significance, which is regarded as the cornerstone of the connected topology network. Most of the connections in the ring structure occur between nearby neurons, and the study of loop supports people to further understand the dynamic behavior of the cyclic network[26]. Therefore, it is essential to investigate the stability of the ring neural network. Low dimensional single-ring structural models with few neurons have been dished[27–29]. A generalized model of the two-neuron single-ring structural network with mixed delays is framed to explore the linear stability of the trivial solution and Hopf bifurcation of a two-neuron network with continuous and discrete delays[27]. A four-neuron ring with self-feedback and delays was considered to investigate linear stability and demonstrate Hopf bifurcations, as well as determine the stability and direction of the Hopf bifurcation[28]. Anti-periodic solutions in a ring of four neurons with multiple delays was proposed to research the existence and exponential stability of anti-periodic solutions of bidirectional associative memory (BAM) neural networks with multiple delays[29]. These models had few neurons and low dimensions whereas actual neural networks are often composed of countless neurons. Therefore, the high-dimensional neural network model is more practical. Single-ring high-dimensional neural networks were probed immediately after[30, 31]. The authors advanced the simplified frequency method for stability and bifurcation of delayed neural networks in ring structure[30]. The authors discussed effects of time delays on stability and Hopf bifurcation in a fractional ring-structured network with arbitrary neurons[31]. However, the actual neural network is composed of multiple rings. Therefore, in order to make the neural network more realistic, this paper promotes the single-ring structure to the multi-ring structure and proposes a double-ring neural network with $n+m$ neurons. Both the double ring and the high dimension are difficult to analyze in such a model.

The contributions of this paper are as follows:

1) A double-ring high-dimensional neural network model is proposed in which the number of neurons in each ring is unequal. This model increases the difficulty of analysis and calculation, the point is more realistic.

2) For the first time, the formula of the Coates' flow graph is used to solve the calculation problem of the high-dimensional feature determinant. The characteristic equation could be directly obtained through the decomposition of the convection diagram, which was clearer and more efficient than the traditional method.

3) Firstly, the dynamic characteristics of a high-dimensional neural network model with two rings sharing a node are studied, as well as the conditions of stability and Hopf bifurcation are obtained.

4) We also consider the effect of the sum of the time delays and the number of neurons on the stability of the neural network. The results show that the dynamics of the neural network are closely related to the sum of the time delays and the number of neurons.

The rest parts of the article are as follows. In Section 2, a high-dimensional double-ring neural network model with multiple time delays is proposed, and the characteristic equation of the model is acquired by the Coates' flow graph formula. In Section 3, the stability of this neural network model is analyzed and the sufficient conditions for the occurrence of Hopf bifurcation are given. In Section 4, some simulation experiments are provided to prove the correctness of our theory. In Section 5, the conclusion is drawn.

2 Model Description

As shown in Figure 1, we consider a neural network model in which two rings share a common node. This model can be described as follows:

$$\begin{cases} \dot{W}_1(t) &= -a_1 W_1(t) + b_{n1} f_n(W_n(t-\tau_{n1})) \\ &\quad + b_{(n+m)1} f_{n+m}(W_{n+m}(t-\tau_{(n+m)1})), \\ \dot{W}_2(t) &= -a_2 W_2(t) + b_{12} f_1(W_1(t-\tau_{12})), \\ \quad\vdots & \\ \dot{W}_n(t) &= -a_n W_n(t) + b_{(n-1)n} f_{n-1}(W_{n-1}(t-\tau_{(n-1)n})), \\ \dot{W}_{n+1}(t) &= -a_{n+1} W_{n+1}(t) + b_{1(n+1)} f_1(W_1(t-\tau_{1(n+1)})), \\ \dot{W}_{n+2}(t) &= -a_{n+2} W_{n+2}(t) + b_{(n+1)(n+2)} f_{n+1}(W_{n+1}(t-\tau_{(n+1)(n+2)})), \\ \quad\vdots & \\ \dot{W}_{n+m}(t) &= -a_{n+m} W_{n+m}(t) \\ &\quad + b_{(n+m-1)(n+m)} f_{n+m-1}(W_{n+m-1}(t-\tau_{(n+m-1)(n+m)})), \end{cases} \tag{1}$$

where $W_i(t)$, $i = 1, 2, \cdots, n+m$ indicate the state of the ith neuron at time t. $a_i > 0$, $i = 1, 2, \cdots, n+m$ are constants. $f_i(\cdot)$, $i = 1, 2, \cdots, n+m$ mean the activation functions. $b_{n1}, b_{(n+m)1}, b_{1(n+1)}$ and $b_{(v-1)v}$, $v = 2, 3, \cdots, n, n+2, n+3, \cdots, n+m$ are constants and

indicate the weight of the connection between two adjacent neurons. $\tau_{n1}, \tau_{(n+m)1}, \tau_{1(n+1)}$ and $\tau_{(v-1)v}$, $v = 2, 3, \cdots, n, n+2, n+3, \cdots, n+m$ are the time delays between two adjacent neurons when passing information.

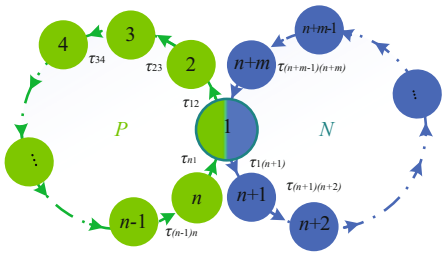

Figure 1 Diagram of the model (1) structure

Firstly, we assume that:

(H1) $f_i(\cdot)$ satisfy $f_i(0) = 0$ and $f_i(\cdot) \in C^1$, $i = 1, 2, \cdots, n+m$. Let

$$\begin{cases} x_c(t) = W_c\left(t - \sum\limits_{c}^{n-1} \tau_{c(c+1)} - \tau_{1(n+1)} - \sum\limits_{p=n+1}^{n+m-1} \tau_{p(p+1)}\right), \\ x_d(t) = W_d\left(t - \sum\limits_{q=1}^{n-1} \tau_{q(q+1)} - \sum\limits_{d}^{n+m-1} \tau_{d(d+1)}\right), \\ x_n(t) = W_n\left(t - \sum\limits_{p=n+1}^{n+m-1} \tau_{p(p+1)} - \tau_{1(n+1)}\right), \\ x_{n+m}(t) = W_{n+m}\left(t - \sum\limits_{p=1}^{n-1} \tau_{p(p+1)}\right), \end{cases}$$

where $c = 1, 2, \cdots, n-1$ and $d = n+1, n+2, \cdots, n+m-1$. We make the following assumption:

(H2) $\tau_{12} + \tau_{23} + \cdots + \tau_{n1} = \tau_{1(n+1)} + \tau_{(n+1)(n+2)} + \cdots + \tau_{(n+m)1} = \tau$, and $\tau_{n1} = \tau_{(n+m)1}$.

Then, the model (1) can be rewritten as:

$$\begin{cases} \dot{x}_1(t) = -a_1 x_1(t) + b_{n1} f_n(x_n(t-\tau)) + b_{(m+n)1} f_{m+n}(x_{m+n}(t-\tau)), \\ \dot{x}_2(t) = -a_2 x_2(t) + b_{12} f_1(x_1(t)), \\ \quad \vdots \\ \dot{x}_n(t) = -a_n x_n(t) + b_{(n-1)n} f_{n-1}(x_{n-1}(t)), \\ \dot{x}_{n+1}(t) = -a_{n+1} x_{n+1}(t) + b_{1(n+1)} f_1(x_1(t)), \\ \dot{x}_{n+2}(t) = -a_{n+2} x_{n+2}(t) + b_{(n+1)(n+2)} f_{n+1}(x_{n+1}(t)), \\ \quad \vdots \\ \dot{x}_{n+m}(t) = -a_{n+m} x_{n+m}(t) + b_{(n+m-1)(n+m)} f_{n+m-1}(x_{n+m-1}(t)). \end{cases} \tag{2}$$

We will search the critical value of the Hopf bifurcation of the model (1) to analyze the stability of the system. Obviously, the origin point is the equilibrium point of the model (2),

and the model (2) is linearized as follows at the trivial equilibrium point:

$$\begin{cases} \dot{x}_1(t) = -a_1x_1(t) + C_{n1}x_n(t-\tau) + C_{(m+n)1}x_{m+n}(t-\tau), \\ \dot{x}_2(t) = -a_2x_2(t) + C_{12}x_1(t), \\ \quad\vdots \\ \dot{x}_n(t) = -a_nx_n(t) + C_{(n-1)n}x_{n-1}(t), \\ \dot{x}_{n+1}(t) = -a_{n+1}x_{n+1}(t) + C_{1(n+1)}x_1(t), \\ \dot{x}_{n+2}(t) = -a_{n+2}x_{n+2}(t) + C_{(n+1)(n+2)}x_{n+1}(t), \\ \quad\vdots \\ \dot{x}_{n+m}(t) = -a_{n+m}x_{n+m}(t) + C_{(n+m-1)(n+m)}x_{n+m-1}(t), \end{cases} \tag{3}$$

where $C_{n1} = b_{n1}f'_n(0)$, $C_{(m+n)1} = b_{(m+n)1}f'_{m+n}(0)$, $C_{1(n+1)} = b_{1(n+1)}f'_1(0)$, $C_{(v-1)v} = b_{(v-1)v}$ $f'_{v-1}(0)$, $v = 2, 3, \cdots, n, n+2, n+3, \cdots, n+m$. We list the characteristic determinant of the model (3) as follows:

$$\det V = \begin{vmatrix} \lambda+a_1 & 0 & 0 & \cdots & 0 & -C_{n1}\mathrm{e}^{-\lambda\tau} & 0 & \cdots & -C_{(n+m)1}\mathrm{e}^{-\lambda\tau} \\ -C_{12} & \lambda+a_2 & 0 & \cdots & 0 & 0 & 0 & \cdots & 0 \\ 0 & -C_{23} & \lambda+a_3 & \cdots & 0 & 0 & 0 & \cdots & 0 \\ \vdots & \vdots & \vdots & \ddots & \vdots & \vdots & \vdots & \cdots & \vdots \\ 0 & 0 & 0 & \cdots & \lambda+a_n & 0 & 0 & \cdots & 0 \\ -C_{1(n+1)} & 0 & 0 & \cdots & 0 & \lambda+a_{n+1} & 0 & \cdots & 0 \\ 0 & 0 & 0 & \cdots & 0 & -C_{(n+1)(n+2)} & \lambda+a_{n+2} & \cdots & 0 \\ \vdots & \vdots & \vdots & \vdots & \vdots & \ddots & \ddots & \ddots & \vdots \\ 0 & 0 & 0 & \cdots & 0 & 0 & 0 & \cdots & \lambda+a_{n+m} \end{vmatrix} = 0.$$

According to previous research results[32], we detect a lemma.

Lemma 2.1 *Define that*

$$\det V = (-1)^{n+m}\sum_{j=1}^{v}(-1)^{n_j}\Lambda_j, \tag{4}$$

where $n+m$ is the order of the determinant and the number of neurons. v is the number of subgraphs G_j, $j = 1, 2, 3$ that represent the simple loop of this $n+m$ neuron (which can not be crossed by itself). n_j denote the number of loops in the graph G_j, $j = 1, 2, 3$ as shown in Figure 2. Λ_j is the product of the weights of the sides of G_j.

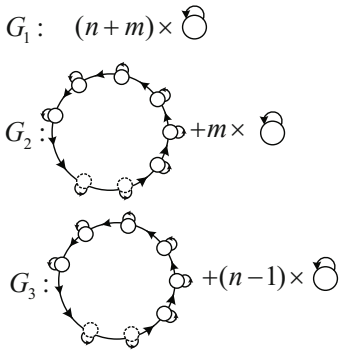

Figure 2 Exploded view of the signal flow diagram

The entire diagram of signal flow structure of the double-ring model is shown in Figure 3.

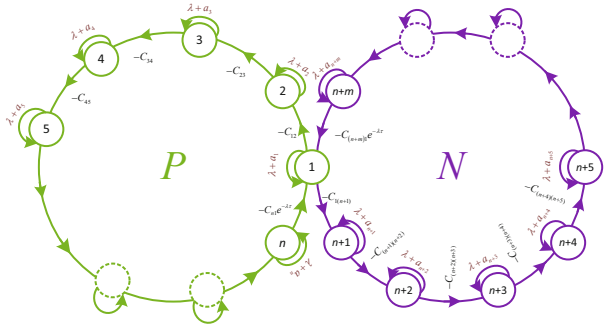

Figure 3 Diagram of signal flow structure

According to Lemma 2.1, we get

$$\begin{cases} \Lambda_1 = (\lambda+a_1)(\lambda+a_2)\cdots(\lambda+a_{n+m}), \\ \Lambda_2 = (-1)^{n+m}(-1)^{m+1}(\lambda+a_{n+1})(\lambda+a_{n+2}) \\ \qquad \cdots(\lambda+a_{n+m})(-1)^n C_{12}C_{23}\cdots C_{(n-1)n}C_{n1}\mathrm{e}^{-\lambda\tau}, \\ \Lambda_3 = (-1)^{n+m}(-1)^n(\lambda+a_2)(\lambda+a_3) \\ \qquad \cdots(\lambda+a_n)(-1)^{m+1}C_{1(n+1)}C_{(n+1)(n+2)}\cdots C_{(n+m-1)(n+m)}C_{(n+m)1}\mathrm{e}^{-\lambda\tau}, \end{cases}$$

so the characteristic equation of the model (3) is

$$\begin{aligned} &\prod_{i=1}^{n+m}(\lambda+a_i) - \mathrm{e}^{-\lambda\tau}\left(\prod_{i=1}^{n-1}C_{i(i+1)}C_{n1}\prod_{i=n+1}^{n+m}(\lambda+a_i)\right) \\ &-\mathrm{e}^{-\lambda\tau}\prod_{i=2}^{n}(\lambda+a_i)\prod_{i=n+1}^{n+m-1}C_{i(i+1)}C_{1(n+1)}C_{(n+m)1} = 0, \end{aligned} \tag{5}$$

which can be expanded as the following:

$$\begin{aligned}&\lambda^{n+m}+A_1\lambda^{n+m-1}+\cdots+A_{n+m}\\&-\mathrm{e}^{-\lambda\tau}\prod_{i=1}^{n-1}C_{i(i+1)}C_{n1}(\lambda^m+B_1\lambda^{m-1}+\cdots+B_m)\\&-\mathrm{e}^{-\lambda\tau}\prod_{i=n+1}^{n+m-1}C_{i(i+1)}C_{1(n+1)}C_{(n+m)1}(\lambda^{n-1}+D_1\lambda^{n-2}+\cdots+D_{n-1})=0,\end{aligned}\tag{6}$$

where

$$\begin{aligned}A_k&=\sum_{1\le i_1<i_2<\cdots<i_k\le n+m}a_{i_1}a_{i_2}\cdots a_{i_k},\\B_k&=\sum_{1\le i_1<i_2<\cdots<i_k\le m}a_{i_1}a_{i_2}\cdots a_{i_k},\\D_k&=\sum_{1\le i_1<i_2<\cdots<i_k\le n-1}a_{i_1}a_{i_2}\cdots a_{i_k}.\end{aligned}$$

From Equation (6), we have

$$\begin{aligned}&\lambda^{n+m}+A_1\lambda^{n+m-1}+\cdots+A_{n+m}\\&-\mathrm{e}^{-\lambda\tau}(E_1\lambda^{\alpha}+E_2\lambda^{\alpha-1}+\cdots+E_{\alpha+1})=0,\end{aligned}\tag{7}$$

where

$$\alpha=\max\{m,n-1\},\quad E_{\alpha+1-r}=\varGamma_1B_{m-r}+\varGamma_2D_{n-1-r},\quad r=0,1,\cdots,\alpha,$$

in which

$$\begin{aligned}\varGamma_1&=\prod_{i=1}^{n-1}C_{i(i+1)}C_{n1},\\\varGamma_2&=\prod_{i=n+1}^{n+m-1}C_{i(i+1)}C_{1(n+1)}C_{(n+m)1},\\D_{n-1-r}&=0,\quad n-1-r<0,\\D_{n-1-r}&=1,\quad n-1-r=0.\end{aligned}$$

Equation (7) can also be expressed as

$$R(\lambda)-\mathrm{e}^{-\lambda\tau}g(\lambda)=0,\tag{8}$$

where

$$\begin{aligned}R(\lambda)&=\lambda^{n+m}+A_1\lambda^{n+m-1}+\cdots+A_{n+m},\\g(\lambda)&=E_1\lambda^{\alpha}+E_2\lambda^{\alpha-1}+\cdots+E_{\alpha+1}.\end{aligned}\tag{9}$$

3 Hopf Bifurcation Analysis

When $\tau\neq0$, by substituting $\lambda=\mathrm{i}\omega$ into (8), we have

$$R(\mathrm{i}\omega)-\mathrm{e}^{-(\mathrm{i}\omega)\tau}g(\mathrm{i}\omega)=0,\tag{10}$$

where

$$\begin{aligned} R(\mathrm{i}\omega) &= (\mathrm{i}\omega)^{n+m} + A_1(\mathrm{i}\omega)^{n+m-1} + \cdots + A_{n+m}, \\ g(\mathrm{i}\omega) &= E_1(\mathrm{i}\omega)^{\alpha} + E_2(\mathrm{i}\omega)^{\alpha-1} + \cdots + E_{\alpha+1}. \end{aligned} \tag{11}$$

Write $R(\mathrm{i}\omega)$ and $g(\mathrm{i}\omega)$ as the real part plus the imaginary part:

$$\begin{aligned} R(\mathrm{i}\omega) &= R_1(\omega) + \mathrm{i}R_2(\omega), \\ g(\mathrm{i}\omega) &= g_1(\omega) + \mathrm{i}g_2(\omega), \end{aligned}$$

where

$$R_1(\omega) = \begin{cases} \omega^{n+m} - A_2\omega^{n+m-2} + A_4\omega^{n+m-4} - A_6\omega^{n+m-6} \\ + \cdots - A_{n+m-2}\omega^2 + A_{n+m}, \quad n+m = 4l, \\ A_1\omega^{n+m-1} - A_3\omega^{n+m-3} + A_5\omega^{n+m-5} - A_7\omega^{n+m-7} \\ + \cdots - A_{n+m-2}\omega^2 + A_{n+m}, \quad n+m = 4l+1, \\ -\omega^{n+m} + A_2\omega^{n+m-2} - A_4\omega^{n+m-4} + A_6\omega^{n+m-6} \\ + \cdots - A_{n+m-2}\omega^2 + A_{n+m}, \ n+m = 4l+2, \\ -A_1\omega^{n+m-1} + A_3\omega^{n+m-3} - A_5\omega^{n+m-5} + A_7\omega^{n+m-7} \\ + \cdots - A_{n+m-2}\omega^2 + A_{n+m}, \quad n+m = 4l+3, \end{cases}$$

$$R_2(\omega) = \begin{cases} -A_1\omega^{n+m-1} + A_3\omega^{n+m-3} - A_5\omega^{n+m-5} + A_7\omega^{n+m-7} \\ + \cdots - A_{n+m-3}\omega^3 + A_{n+m-1}\omega, \quad n+m = 4l, \\ \omega^{n+m} - A_2\omega^{n+m-2} + A_4\omega^{n+m-4} - A_6\omega^{n+m-6} \\ + \cdots - A_{n+m-3}\omega^3 + A_{n+m-1}\omega, \quad n+m = 4l+1, \\ A_1\omega^{n+m-1} - A_3\omega^{n+m-3} + A_5\omega^{n+m-5} - A_7\omega^{n+m-7} \\ + \cdots - A_{n+m-3}\omega^3 + A_{n+m-1}\omega, \quad n+m = 4l+2, \\ -\omega^{n+m} + A_2\omega^{n+m-2} - A_4\omega^{n+m-4} + A_6\omega^{n+m-6} \\ + \cdots - A_{n+m-3}\omega^3 + A_{n+m-1}\omega, \quad n+m = 4l+3, \end{cases}$$

$$g_1(\omega) = \begin{cases} E_1\omega^{\alpha} - E_3\omega^{\alpha-2} + E_5\omega^{\alpha-4} + \cdots - E_{\alpha-1}\omega^2 + E_{\alpha+1}, \quad \alpha = 4l, \\ E_2\omega^{\alpha-1} - E_4\omega^{\alpha-3} + E_6\omega^{\alpha-5} + \cdots - E_{\alpha-1}\omega^2 + E_{\alpha+1}, \quad \alpha = 4l+1, \\ -E_1\omega^{\alpha} + E_3\omega^{\alpha-2} - E_5\omega^{\alpha-4} + \cdots - E_{\alpha-1}\omega^2 + E_{\alpha+1}, \quad \alpha = 4l+2, \\ -E_2\omega^{\alpha-1} + E_4\omega^{\alpha-3} - E_6\omega^{\alpha-5} + \cdots - E_{\alpha-1}\omega^2 + E_{\alpha+1}, \quad \alpha = 4l+3, \end{cases}$$

$$g_2(\omega) = \begin{cases} -E_2\omega^{\alpha-1} + E_4\omega^{\alpha-3} - E_6\omega^{\alpha-5} + \cdots - E_{\alpha-2}\omega^3 + E_{\alpha}\omega, \quad \alpha = 4l, \\ E_1\omega^{\alpha} - E_3\omega^{\alpha-2} + E_5\omega^{\alpha-4} + \cdots - E_{\alpha-2}\omega^3 + E_{\alpha}\omega, \quad \alpha = 4l+1, \\ E_2\omega^{\alpha-1} - E_4\omega^{\alpha-3} + E_6\omega^{\alpha-5} + \cdots - E_{\alpha-2}\omega^3 + E_{\alpha}\omega, \quad \alpha = 4l+2, \\ -E_1\omega^{\alpha} + E_3\omega^{\alpha-2} - E_5\omega^{\alpha-4} + \cdots - E_{\alpha-2}\omega^3 + E_{\alpha}\omega, \quad \alpha = 4l+3, \end{cases}$$

in which $l = 0, 1, \cdots$. Then (10) can be written as:

$$R_1(\omega) + \mathrm{i}R_2(\omega) - \mathrm{e}^{-\lambda\tau}[g_1(\omega) + \mathrm{i}g_2(\omega)] = 0. \tag{12}$$

Separating the real and imaginary parts, we can get:

$$\begin{aligned} R_1(\omega) &= g_1(\omega)\cos\omega\tau + g_2(\omega)\sin\omega\tau, \\ R_2(\omega) &= -g_1(\omega)\sin\omega\tau + g_2(\omega)\cos\omega\tau. \end{aligned} \tag{13}$$

Adding the squares of both sides of (13), we can obtain that

$$R_1^2(\omega) + R_2^2(\omega) = g_1^2(\omega) + g_2^2(\omega),$$

which is

$$\omega^{2(n+m)} + K_1\omega^{2(n+m-1)} + K_2\omega^{2(n+m-2)}\cdots + K_{n+m} = 0, \tag{14}$$

where K_i, $i = 1, 2, \cdots, n+m$ are the coefficients and available when entering specific values. Let $z = \omega^2$, we have

$$z^{n+m} + K_1 z^{n+m-1} + K_2 z^{n+m-2}\cdots + K_{n+m} = 0. \tag{15}$$

Let

$$h(z) = z^{n+m} + K_1 z^{n+m-1} + K_2 z^{n+m-2}\cdots + K_{n+m}.$$

Lemma 3.1 *If $K_{n+m} < 0$, $\pm\mathrm{i}\omega_0$ are the two pure virtual roots of* (15) *at $\tau = \tau_j$.*

Proof If $K_{n+m} < 0$, then $h(0) = K_{n+m} < 0$ and $\lim_{z\to+\infty} h(z) = +\infty$, there is at least one number z_0 satisfies $h(z_0) = 0$. Through $z = \omega^2$, we can obtain $\pm\mathrm{i}\omega_0$ are the two pure virtual roots of (7). The proof is completed. ∎

We make an assumption that (15) has the $n+m$ positive roots $z_1, z_2, \cdots, z_{n+m}$, then (14) has the following $n+m$ positive roots:

$$\omega_1 = \sqrt{z_1}, \quad \omega_2 = \sqrt{z_2}, \quad \cdots, \quad \omega_{n+m} = \sqrt{z_{n+m}}.$$

From (13) we can further get

$$\cos\omega_\upsilon\tau = \frac{g_1(\omega_\upsilon)R_1(\omega_\upsilon) + g_2(\omega_\upsilon)R_2(\omega_\upsilon)}{{g_1}^2(\omega_\upsilon) + {g_2}^2(\omega_\upsilon)}, \quad \upsilon = 1, 2, \cdots, n+m,$$

so we have

$$\begin{aligned} &{\tau_\upsilon}^{(j)} = \frac{1}{\omega_\upsilon}\left\{\arccos\frac{g_1(\omega_\upsilon)R_1(\omega_\upsilon) + g_2(\omega_\upsilon)R_2(\omega_\upsilon)}{{g_1}^2(\omega_\upsilon) + {g_2}^2(\omega_\upsilon)} + 2j\pi\right\}, \\ &\upsilon = 1, 2, \cdots, n+m, \quad j = 0, 1, \cdots, \end{aligned} \tag{16}$$

then $\pm\mathrm{i}\omega_\upsilon$ is a pair of purely imaginary root of Equation (7) when $\tau = {\tau_\upsilon}^{(j)}$. We define

$$\tau_0 = {\tau_{\upsilon 0}}^{(0)} = \min_{\upsilon\in\{1,2,\cdots,n+m\}}\left\{{\tau_\upsilon}^{(0)}\right\}, \quad \omega_0 = \omega_{\upsilon 0}. \tag{17}$$

If $\lambda(\tau) = \varrho(\tau) + \mathrm{i}\omega(\tau)$ is the root of (7) satisfied $\varrho({\tau_\upsilon}^{(j)}) = 0$ and $\omega({\tau_\upsilon}^{(j)}) = \omega_0$ ($\upsilon = 1, 2, \cdots, n+m, j = 0, 1, \cdots$), we deduce:

Lemma 3.2 *If $K_i > 0$ $(i = 1, 2, \cdots, n+m-1)$, then*

$$\mathrm{Re}\left[\frac{d\lambda}{d\tau}\right]\Bigg|_{\tau=\tau_0} \neq 0.$$

Proof Deriving (8) with respect to τ, we can get

$$\frac{d\lambda}{d\tau} = \frac{\lambda \mathrm{e}^{-\lambda\tau} g(\lambda)}{R'(\lambda) + \tau \mathrm{e}^{-\lambda\tau} g(\lambda) - \mathrm{e}^{-\lambda\tau} g'(\lambda)}. \tag{18}$$

For the convenience of calculation, we find the reciprocal of (18):

$$\left(\frac{d\lambda}{d\tau}\right)^{-1} = \frac{R'(\lambda) + \tau \mathrm{e}^{-\lambda\tau} g(\lambda) - \mathrm{e}^{-\lambda\tau} g'(\lambda)}{\lambda \mathrm{e}^{-\lambda\tau} g(\lambda)} = \frac{\tau}{\lambda} + \frac{g'(\lambda) - \mathrm{e}^{\lambda\tau} R'(\lambda)}{\lambda g(\lambda)}. \tag{19}$$

Substituting $\lambda = \mathrm{i}\omega_0$, we have

$$\begin{aligned}
\mathrm{Re}\left[\frac{d\lambda}{d\tau}\right]^{-1}\Bigg|_{\tau=\tau_0} &= \mathrm{Re}\left[\frac{g'(\lambda) - \mathrm{e}^{\lambda\tau} R'(\lambda)}{\lambda g(\lambda)}\right]^{-1} \\
&= \frac{g'(\mathrm{i}\omega_0) - R'(\mathrm{i}\omega_0)(\cos\omega_0\tau + \mathrm{i}\sin\omega_0\tau)}{(\mathrm{i}\omega_0) g(\mathrm{i}\omega_0)} \\
&= \frac{\omega_0^2 h'(\omega_0^2)}{\omega_0^2 (g_1^2(\omega_0) + g_2^2(\omega_0))} \\
&= \frac{h'(\omega_0^2)}{g_1^2(\omega_0) + g_2^2(\omega_0)}.
\end{aligned}$$

Thus,

$$\mathrm{sign}\left\{\mathrm{Re}\left[\frac{d\lambda}{d\tau}\right]\Big|_{\tau=\tau_0}\right\} = \mathrm{sign}\left\{\mathrm{Re}\left[\frac{d\lambda}{d\tau}\right]^{-1}\Bigg|_{\tau=\tau_0}\right\} = \mathrm{sign}\left\{\frac{h'(\omega_0^2)}{g_1^2(\omega_0) + g_2^2(\omega_0)}\right\}.$$

Since $K_i > 0$ $(i = 1, 2, \cdots, n+m-1)$, then $h'(\omega_0^2) > 0$. Together with $g_1^2(\omega_0) + g_2^2(\omega_0) > 0$, the sign is positive. The proof is completed. ∎

When $\tau = 0$, Equation (7) becomes

$$\begin{aligned}
&\lambda^{n+m} + A_1\lambda^{n+m-1} + \cdots + (A_{n+m-\alpha} + E_1)\lambda^{\alpha} \\
&+(A_{n+m-\alpha+1} + E_2)\lambda^{\alpha-1} + \cdots + (A_{n+m} + E_{\alpha+1}) = 0.
\end{aligned} \tag{20}$$

Namely,

$$\lambda^{n+m} + F_1\lambda^{n+m-1} + \cdots + F_{n+m-\alpha}\lambda^{\alpha} + F_{n+m-\alpha+1}\lambda^{\alpha-1} + \cdots + F_{n+m} = 0, \tag{21}$$

where $F_i = A_i$, $i = 1, 2, \cdots, n+m-\alpha-1$ and $F_j = A_j + E_\iota$, $j = n+m-\alpha, n+m-\alpha+1, \cdots, n+m$; $\iota = 1, 2, \cdots, \alpha+1$ are coefficients. They are available when entering specific values.

We define that

$$\begin{aligned}
&\Delta_1 = F_1{=}A_1,\\
&\Delta_2 = \begin{vmatrix} F_1 & F_3 \\ 1 & F_2 \end{vmatrix},\\
&\Delta_3 = \begin{vmatrix} F_1 & F_3 & F_5 \\ 1 & F_2 & F_4 \\ 0 & F_1 & F_3 \end{vmatrix},\\
&\qquad\vdots\\
&\Delta_{n+m} = \begin{vmatrix}
F_1 & F_3 & F_5 & \cdots & F_{2(n+m-\alpha)-1} & \cdots & 0 \\
1 & F_2 & F_4 & \cdots & F_{2(n+m-\alpha)-2} & \cdots & 0 \\
0 & F_1 & F_3 & \cdots & \vdots & \cdots & 0 \\
0 & 1 & F_2 & \cdots & F_{n+m-\alpha} & \cdots & 0 \\
\vdots & \vdots & \vdots & \vdots & \ddots & \vdots & \vdots \\
0 & 0 & 0 & \cdots & F_{n+m-3} & F_{n+m-1} & 0 \\
0 & 0 & 0 & 0 & \cdots & F_{n+m-2} & F_{n+m}
\end{vmatrix}.
\end{aligned} \tag{22}$$

We make the following assumption:

(H3) $\triangle_i > 0$, $i = 1, 2, \cdots, n+m$.

According to the Routh-Hurwitz criterion, we deduce that if (H3) holds, (21) has $n+m$ roots with negative real parts when $\tau = 0$.

Remark 3.3 Hopf bifurcation is the birth of a limit cycle from an equilibrium in dynamical systems generated by ordinary differential equation when the equilibrium changes stability via a pair of purely imaginary eigenvalues. The bifurcation can be supercritical or subcritical, resulting in stable or unstable limit cycle, respectively. We maintain that the system is stable in the initial state, and the critical value of the system from stable to unstable after adding time delays is our requirement.

Remark 3.4 Since we use the sum of time delays as the the parameter to study bifurcation, we ensure that the system is stable without time delays. When $\tau = 0$, the characteristic equation of the system is transformed into a polynomial equation, and the distribution of the roots of the polynomial equation is usually determined by Hurwitz criterion[33–35]. This paper deals with high-dimensional systems, which will be more complex with nonlinear methods, such as Lyapunov. Therefore, we usually use Hurwitz criterion to solve the local stability problem and obtain the stability threshold of the system.

By Lemmas 2.1 3.1 and 3.2, we can draw the following conclusions:

Theorem 3.5 *If* (H1)–(H3) *hold, we have:*

(i) *Model* (1) *is locally asymptotically stable for all* $\tau \in [0, \tau_0)$ *at the equilibrium point.*

(ii) *Model* (1) *begets a Hopf bifurcation at the equilibrium point when* $\tau = \tau_0$*, and becomes unstable when* $\tau > \tau_0$*.*

4 Numerical Simulations

In this section, we use two numerical examples to prove the correctness of our previous theoretical results. Some parameter values on the model (1) are given to observe the waveforms and phase diagrams to see the accuracy of the results.

4.1 Example 1

We take $n = 4$, $m = 5$, and $f(\cdot) = \tanh(\cdot)$ in this example. Then, we have

$$\begin{cases} \dot{W}_1(t) = -a_1 W_1(t) + b_{41}\tanh(W_4(t-\tau_{41})) + b_{91}\tanh(W_9(t-\tau_{91})), \\ \dot{W}_2(t) = -a_2 W_2(t) + b_{12}\tanh(W_1(t-\tau_{12})), \\ \dot{W}_3(t) = -a_3 W_3(t) + b_{23}\tanh(W_2(t-\tau_{23})), \\ \dot{W}_4(t) = -a_4 W_4(t) + b_{34}\tanh(W_3(t-\tau_{34})), \\ \dot{W}_5(t) = -a_5 W_5(t) + b_{15}\tanh(W_1(t-\tau_{15})), \\ \dot{W}_6(t) = -a_6 W_6(t) + b_{56}\tanh(W_5(t-\tau_{56})), \\ \dot{W}_7(t) = -a_7 W_7(t) + b_{67}\tanh(W_6(t-\tau_{67})), \\ \dot{W}_8(t) = -a_8 W_8(t) + b_{78}\tanh(W_7(t-\tau_{78})), \\ \dot{W}_9(t) = -a_9 W_9(t) + b_{89}\tanh(W_8(t-\tau_{89})). \end{cases} \tag{23}$$

The values of each parameter in the model (23) are as Table 1.

Table 1 Parameters of the model (23) are given in Example 1

a_1	a_2	a_3	a_4	a_5	a_6	a_7	a_8	a_9	
1.2	1.2	1.2	1.2	1.2	1.2	1.2	1.2	1.2	
b_{12}	b_{23}	b_{34}	b_{41}	b_{15}	b_{56}	b_{67}	b_{78}	b_{89}	b_{91}
−0.8	1.2	1.2	1.2	−0.8	1.2	1.2	1.2	1.2	1.2

From (16), $\tau_0 = 4.2391$ can be generated. Figure 4 shows that when $\tau = 4.1 < \tau_0 = 4.2391$, the model (23) is asymptotically stable near the equilibrium point. In contrast, as shown in Figure 5, when $\tau = 4.3 > \tau_0 = 4.2391$, the model (23) becomes unstable, and Hopf bifurcation is generated. Figure 6 clearly shows that when $\tau < \tau_0$, the curve converges to the limit point. Conversely, as shown in Figure 7, when $\tau > \tau_0$, the limit circle of the curve appears, which means that the Hopf bifurcation occurs. The results obtained by simulation are in accordance with Theorem 3.5.

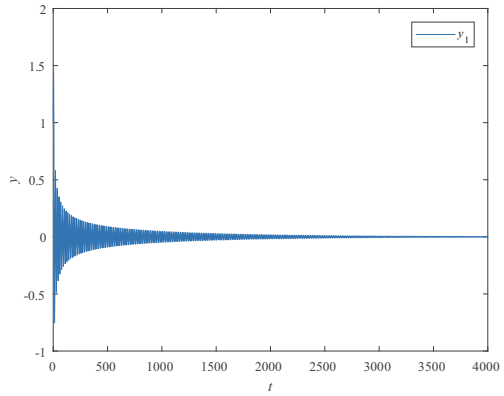

Figure 4 Waveform plot of the model (23) with $\tau = 4.1 < \tau_0 = 4.2391$. It is convergent at the origin $O(0, 0, \cdots, 0)_{1\times 9}$

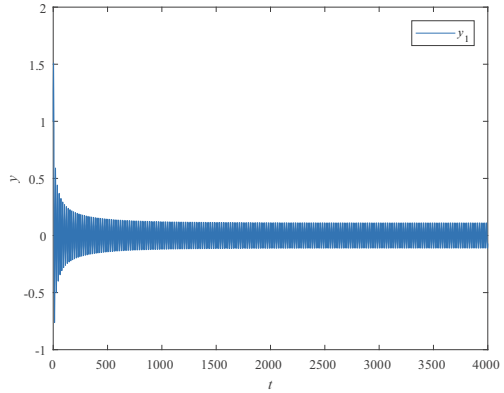

Figure 5 Waveform plot of the model (23) with $\tau = 4.3 > \tau_0 = 4.2391$. It is oscillating at the origin $O(0, 0, \cdots, 0)_{1\times 9}$

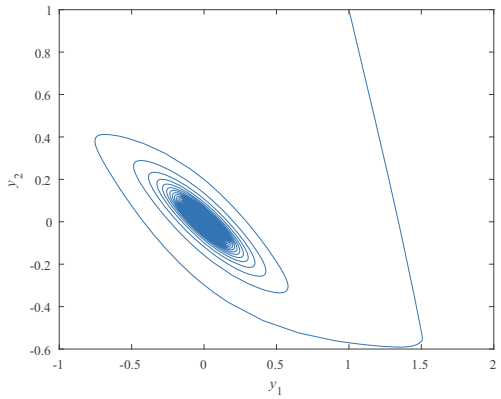

Figure 6 Phase portrait of the model (23) with $\tau = 4.1 < \tau_0 = 4.2391$. The track returns to equilibrium $O(0, 0, \cdots, 0)_{1\times 9}$

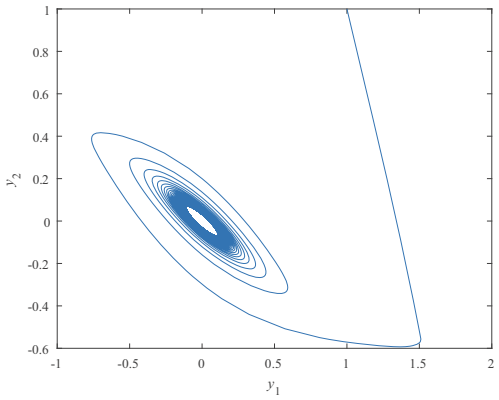

Figure 7 Phase portrait of the model (23) with $\tau = 4.3 > \tau_0 = 4.2391$. The limit cycle appears at the equilibrium $O(0, 0, \cdots, 0)_{1\times 9}$

From Table 2, we find that the value of τ_0 decreases and the stability domain of the model shrinks as the number of neurons increases.

Table 2 The influence of numbers of neurons when the number of neurons on each ring is different

n	m	Bifurcation point τ_0
3	4	4.3130
4	5	4.2391
5	6	4.1003
6	7	3.9109
7	8	3.6807

4.2 Example 2

In Example 1 we discussed the situation of unequal number of neurons on each ring. Unlike it, in Example 2, we study the case where the number of neurons on each ring is equal. We take $n = 6$, $m = 5$, and $f(\cdot) = \tanh(\cdot)$. Then, we have

$$\begin{cases} \dot{W}_1(t) &= -a_1 W_1(t) + b_{61}\tanh(W_6(t-\tau_{61})) + b_{(11)1}\tanh(W_9(t-\tau_{(11)1})), \\ \dot{W}_2(t) &= -a_2 W_2(t) + b_{12}\tanh(W_1(t-\tau_{12})), \\ \dot{W}_3(t) &= -a_3 W_3(t) + b_{23}\tanh(W_2(t-\tau_{23})), \\ \dot{W}_4(t) &= -a_4 W_4(t) + b_{34}\tanh(W_3(t-\tau_{34})), \\ \dot{W}_5(t) &= -a_5 W_5(t) + b_{45}\tanh(W_4(t-\tau_{45})), \\ \dot{W}_6(t) &= -a_6 W_6(t) + b_{56}\tanh(W_5(t-\tau_{56})), \\ \dot{W}_7(t) &= -a_7 W_7(t) + b_{17}\tanh(W_1(t-\tau_{17})), \\ \dot{W}_8(t) &= -a_8 W_8(t) + b_{78}\tanh(W_7(t-\tau_{78})), \\ \dot{W}_9(t) &= -a_9 W_9(t) + b_{89}\tanh(W_8(t-\tau_{89})), \\ \dot{W}_{10}(t) &= -a_{10} W_{10}(t) + b_{9(10)}\tanh(W_9(t-\tau_{9(10)})), \\ \dot{W}_{11}(t) &= -a_{11} W_{11}(t) + b_{(10)(11)}\tanh(W_{10}(t-\tau_{(10)(11)})). \end{cases} \tag{24}$$

The values of each parameter in the model (24) are as the following Table 3.

Table 3 The values of each parameter in the model (24) are given in Example 2

a_1	a_2	a_3	a_4	a_5	a_6	a_7	a_8	a_9	a_{10}	a_{11}	
1.2	1.2	1.2	1.2	1.2	1.2	1.2	1.2	1.2	1.2	1.2	
b_{12}	b_{23}	b_{34}	b_{45}	b_{56}	b_{61}	b_{17}	b_{78}	b_{89}	$b_{9(10)}$	$b_{(10)(11)}$	$b_{(11)1}$
−0.8	1.2	1.2	1.2	1.2	1.2	−0.8	1.2	1.2	1.2	1.2	1.2

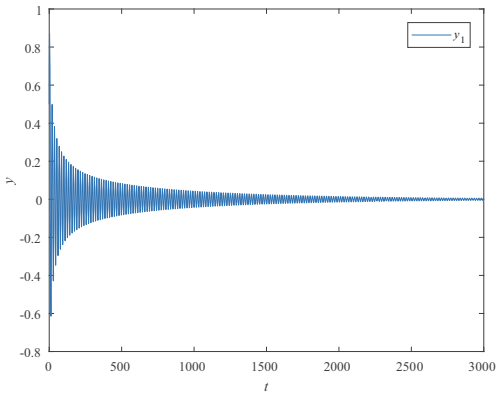

Figure 8 Waveform plots of the model (24) with $\tau = 3.25 < \tau_0 = 3.4106$. It is convergent at the origin $O(0, 0, \cdots, 0)_{1\times 11}$

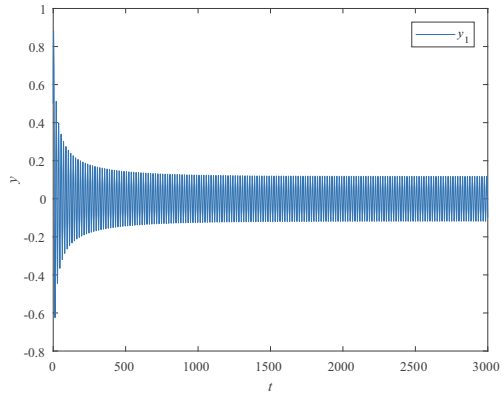

Figure 9 Waveform plots of the model (24) with $\tau = 3.5 > \tau_0 = 3.4106$. It is oscillating at the origin $O(0, 0, \cdots, 0)_{1\times 11}$

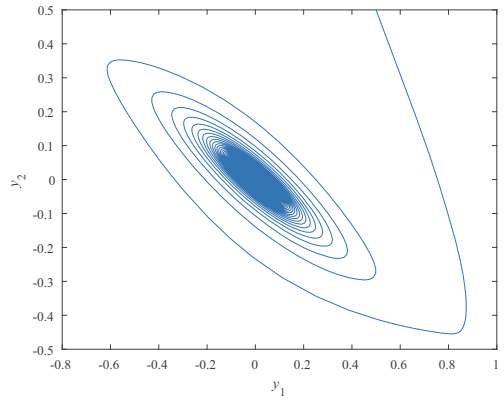

Figure 10 Phase portraits of the model (24) with $\tau = 3.25 < \tau_0 = 3.4106$. The track returns to equilibrium $O(0, 0, \cdots, 0)_{1\times 11}$

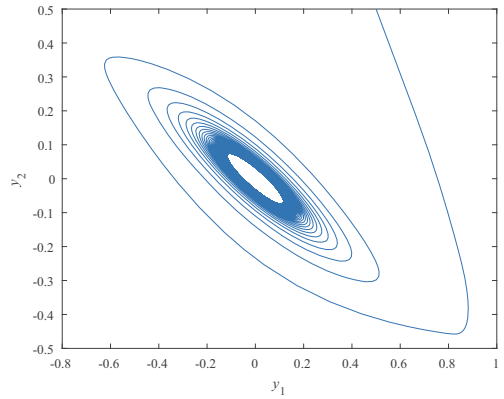

Figure 11 Phase portraits of the model (24) with $\tau = 3.5 > \tau_0 = 3.4106$. The limit cycle appears at the equilibrium $O(0, 0, \cdots, 0)_{1\times 11}$

By calculating according (16), $\tau_0 = 4.2391$ can be obtained. According to Theorem 3.5, the model (24) is asymptotically stable near the equilibrium point when $\tau = 3.25 < \tau_0 = 3.4106$. Model (24) becomes unstable, and Hopf bifurcation is generated around the balance when $\tau = 3.5 > \tau_0 = 3.4106$. In Figures 8–11, Figures 8 and 10 show that the curve converges to the equilibrium point when $\tau < \tau_0$. Contrastly, as shown in Figures 9 and 11, the waveform diagram is divergent, and the limit diagram appears in the phase diagram when $\tau > \tau_0$, which means that the Hopf bifurcation occurs. The results are in accordance with Theorem 3.5.

From Table 4, we find the same as Table 2, the value of τ_0 decreases and the stability area of the model shrinks when the number of neurons increases.

Table 4 The influence of numbers of neurons when the number of neurons on each ring is the same

n	m	Bifurcation point τ_0
5	4	3.4880
6	5	3.4106
7	6	3.2698
8	7	3.0791
9	8	2.8480

Remark 4.1 Excitation and inhibition refer to two basic neural processes. The excitement process is manifested as the activation or enhancement of certain activities, while the inhibition process is manifested as the cessation or weakening of biological activities. Experiments have shown that the excitation and inhibition of the nervous system depends on the nature of the chemical transmitters released by presynaptic cells in the process of presynaptic transmission. The positive parameter here actually represents the excitation state, while the negative parameter represents the inhibition state, which is a negative feedback situation.

5 Conclusions

In this paper, we mainly study the stability and Hopf bifurcation of the double-loop high-dimensional neural network model. The conditions for the occurrence of bifurcation are solved by using the method of Coates' flow graph formula. The correctness of the theory is verified through the numerical simulation. The system becomes obviously unstable at the bifurcation point when the parameter is greater than the critical value. At the same time, we find that the number of neurons has a great influence on the stability area of the system. The greater the number of neurons, the worse the stability of the system. This article enriches the dynamics of high-dimensional neural network models.

In the future, we will be engaged in the neural network model of multi-ring sharing a node. The high-dimensional neural network model of two-way connection is also the direction of our research.

References

[1] Lian D, Existence and global exponential stability of pseudo almost periodic solutions of a general delayed BAM neural networks, *Journal of Systems Science and Complexity*, 2018, **31**(3): 608–620.

[2] Mai V T and Dinh C H, Robust finite-time stability and stabilization of a class of fractional-order switched nonlinear systems, *Journal of Systems Science and Complexity*, 2019, **32**(6): 1479–1497.

[3] Ralph E H, Donald M Q, Carolyn M M, et al., Cortical instability and the mechanism of mania: A neural network simulation and perceptual test, *Biol. Psychiatry*, 2001, **49**(6): 500–509.

[4] Jefferson M F, Pendleton N, Lucas C P, et al., Evolution of artificial neural network architecture Prediction of depression after mania, *Methods Inf. Med.*, 1998, **37**(3): 220–225.

[5] Zieglgansberger W and Tolle T R, The pharmacology of pain signalling, *Curr. Opin. Neurobiol.*, 1993, **3**(4): 611–618.

[6] Hopfield J J, Neurons with graded response have collective computational properties like those of two-state neurons, *Proc. Natl. Acad. Sci. U. S. A.*, 1984, **81**(10): 3088–3092.

[7] Duan L, Shi M, and Huang L H, New results on finite-/fixed-time synchronization of delayed diffusive fuzzy HNNs with discontinuous activations, *Fuzzy Sets Syst.*, 2020, 10.1016/j.fss.2020.04.016.

[8] Luo S H, Li S B, and Tajaddodianfar F, Chaos and nonlinear feedback control of the arch micro-electro-mechanical system, *Journal of Systems Science and Complexity*, 2018, **31**(6): 1510–1524.

[9] Zhang R, Ding G Y, Zhang F Q, et al., The application of intelligent algorithm and pulse coupled neural network in medical image process, *J. Med. Imaging Health Inform.*, 2017, **7**(4): 775–779.

[10] Secco J, Poggio M, and Corinto F, Supervised neural networks with memristor binary synapses, *Int. J. Circuit Theory Appl.*, 2018, **46**(1): 221–233.

[11] Song Y D, Lewis F L, and Polycarpou M, Guest editorial special issue on new developments in neural network structures for signal processing, autonomous decision, and adaptive control, *IEEE Trans. Neural Netw. Learn. Syst.*, 2017, **28**(3): 494–499.

[12] Zhang P, Li C, and Huang T, Forgetting memristor based neuromorphic system for pattern training and recognition, *Neurocomputing*, 2017, **222**(222): 47–53.

[13] Huang C D, Nie X B, Zhao X, et al., Novel bifurcation results for a delayed fractional-order quaternion-valued neural network, *Neural Netw.*, 2019, **117**: 67–93.

[14] Kais B, A new class of neural networks and its applications, *Neurocomputing*, 2017, **249**: 28–47.

[15] Xue H B and Zhang J Y, Robust exponential stability of switched interval interconnected systems with unbounded delay, *Journal of Systems Science and Complexity*, 2017, **30**(6): 1316–1331.

[16] Ge J H and Xu J, Stability and Hopf bifurcation on four-neuron neural networks with inertia and multiple delays, *Neurocomputing*, 2018, **287**: 34–44.

[17] Duan L, Huang L H, Guo Z Y, et al., Periodic attractor for reaction-diffusion high-order Hopfield neural networks with time-varying delays, *Comput. Math. with Appl.*, 2016, **73**(2): 233–245.

[18] Duan L, Wei H, and Huang L H, Finite-time synchronization of delayed fuzzy cellular neural networks with discontinuous activations, *Fuzzy Sets Syst.*, 2018, **361**: 56–70.

[19] Mao X C and Wang Z H, Stability, bifurcation, and synchronization of delay-coupled ring neural networks, *Nonlinear Dyn.*, 2016, **84**(2): 1063–1078.

[20] Liu B, Hill D J, Zhang C F, et al., Stabilization of discrete-time dynamical systems under event-triggered impulsive control with and without time-delays, *Journal of Systems Science and Complexity*, 2018, **31**(1): 130–146.

[21] Jiang D P and Zhang K Z, Observability of boolean control networks with time-variant delays in

states, *Journal of Systems Science and Complexity*, 2018, **31**(2): 436–445.

[22] Zhang Q J, Wu X Q, and Liu J, Pinning synchronization of discrete-time complex networks with different time-varying delays, *Journal of Systems Science and Complexity*, 2019, **32**(6): 1560–1571.

[23] Masaki K, Multistate vector product hopfield neural networks, *Neurocomputing*, 2018, **272**: 425–431.

[24] Reza M S and Saeed F, On a discrete-time-delayed Hopfield neural network with ring structures and different internal decays: Bifurcations analysis and chaotic behavior, *Neurocomputing*, 2015, **151**: 188–195.

[25] Collins J J and Stewart I, A group-theoretic approach to rings of coupled biological oscillators, *Biol. Cybern.*, 1994, **71**(2): 95–103.

[26] Zhang C R, Sui Z Z, and Li H P, Equivariant bifurcation in a coupled complex-valued neural network rings, *Chaos Solitons Fractals*, 2017, **98**: 22–30.

[27] Bi P and Hu Z X, Hopf bifurcation and stability for a neural network model with mixed delays, *Appl. Math. Comput.*, 2012, **218**(12): 6748–6761.

[28] Hu H J and Huang L H, Stability and Hopf bifurcation analysis on a ring of four neurons with delays, *Appl. Math. Comput.*, 2009, **213**(2): 587–599.

[29] Xu C J and Zhang Q M, Anti-periodic solutions in a ring of four neurons with multiple delays, *Int. J. Comput. Math.*, 2015, **92**(5): 1086–1100.

[30] Cai T Y, Zhang H G, and Yang F S, Simplified frequency method for stability and bifurcation of delayed neural networks in ring structure, *Neurocomputing*, 2013, **121**: 416–422.

[31] Huang C D, Cao J D, Xiao M, et al., Effects of time delays on stability and Hopf bifurcation in a fractional ring-structured network with arbitrary neurons, *Commun. Nonlinear Sci. Numer. Simul.*, 2018, **57**: 1–13.

[32] Desoer C A, The optimum formula for the gain of a flow graph or a simple derivation of Coates' formula, *Proceedings of the IRE*, 1960, **48**: 883–889.

[33] Cheng Z S, Xie K H, Wang T S, et al., Stability and Hopf bifurcation of three-triangle neural networks with delays, *Neurocomputing*, 2018, **322**: 206–215.

[34] Li L, Wang Z, Li Y X, et al., Hopf bifurcation analysis of a complex-valued neural network model with discrete and distributed delays, *Appl. Math. Comput.*, 2018, **330**: 152–169.

[35] Wang T S, Cheng Z S, Bu R, et al., Stability and Hopf bifurcation analysis of a simplified six-neuron tridiagonal two-layer neural network model with delays, *Neurocomputing*, 2019, **332**: 203–214.